MICROWAVE MODE COUPLING ABOVE ACTIVE REGIONS AS A CORONAL DENSITY DIAGNOSTIC

Jeongwoo Lee, Stephen M. White and M. R. Kundu
Astronomy Department, University of Maryland, College Park, MD 20742

Zoran Mikić
Science Applications International Corporation, San Diego, CA 92121

A. N. McClymont
Institute for Astronomy, University of Hawaii, Honolulu, HI 96822

Abstract. It is well recognized that the phenomenon of depolarization (the conversion of polarized radio emission into unpolarized emission) of microwaves over solar active regions can be used to infer the coronal electron density once the coronal magnetic field is known. In this paper we explore this technique using an active region for which we have excellent radio data showing depolarization at two frequencies, and for which we have an excellent magnetic field model which has been tested against observations. We show that this technique for obtaining coronal densities is very sensitive to a number of factors. When Cohen's (1960) theory where depolarization is due to magnetic field rotation alone is used, the result is particularly sensitive to the location of the surface on which the magnetic field is orthogonal to the line of sight. Depending on whether we take into account the presence of electric currents in the photosphere or not, their extrapolation into the corona can result in very different heights being deduced for the location of the depolarization strip, and this changes the density which is then deduced from the depolarization condition. Such extreme sensitivity to the magnetic field model requires that field extrapolations be able to accurately predict the polarity of magnetic fields up to coronal heights as high as $\sim 10^5$ km in order to exploit depolarization as a density diagnostic.

Key words: Corona, Magnetic Fields, Polarization, Mode Coupling

1. Introduction

The ability to measure the fundamental physical properties of the solar atmosphere, such as temperature, density and magnetic field, is essential to progress in understanding the processes which occur there. In this paper we investigate a method for measuring electron number densities in the solar corona. At present, the only viable technique for measuring electron densities in the non–flaring corona directly involves radio emission, since other techniques (optical forbidden lines, EUV and X–ray lines) actually measure the number density of a particular charge state of a particular element, rather than the electron number density (the non–flaring corona does not produce enough continuum emission at short wavelengths for it to be useful), and the (unknown and possibly spatially variable) abundance of this particular state must be assumed in order to convert the measurements to electron densities.

Radio observations provide several diagnostics of electron density. The simplest involves the measurement of free–free (bremsstrahlung) emission, which is produced by the collisions of electrons with protons and α particles. The observed free–free emission is thus generally dominated by regions of high density which occur at low altitudes in active regions. A second technique can, in principle, be exploited at somewhat greater heights where the free–free emission is too weak to be very useful, and this is the technique addressed in this paper. This technique involves observation of the locations at which radio emission from the underlying active region becomes depolarized. In an ionized plasma such as the Sun's corona, the two natural modes of the plasma are circularly polarized everywhere except for a narrow range of propagation angles orthogonal to the local magnetic field. Since electrons interact more strongly with one mode (the mode which is polarized in the same sense that the electron gyrates about the magnetic field, labeled the X mode) than the other (the O mode), the emission is generally preferentially circularly polarized in one particular sense (X mode) when it leaves the emission region. The X and O modes generally propagate independently of one other, and hence the polarization is unchanged during propagation, if the medium is uniform. However, due to the inhomogeneous nature of the corona, coupling between the two modes may occur if their refractive indices become similar (which depends on the frequency, magnetic field and density; e.g., Cohen, 1960). One particular outcome of mode coupling is the complete depolarization of the emission, and this case has the potential to be a valuable diagnostic.

Kundu and Alissandrakis (1984) exploited this diagnostic using 5 GHz polarization observations made with the Westerbork Synthesis Radio Telescope on several consecutive days. Depolarization corresponds to a specific relationship between density and magnetic field being satisfied. Kundu and Alissandrakis (1984) assumed an electron density of $\sim 10^8$ cm^{-3}, and for a dipole configuration for the magnetic field they derived a magnetic field strength of 10–20 G in the depolarization layer. Gelfreikh, Peterova, and Ryabov (1987) used multiple frequencies and were able to derive the coronal field strength as a function of height. Most recently, Alissandrakis et al. (1996) make use of a potential field (PF) extrapolation to determine the magnetic field, and then use depolarization observations to derive the coronal density. The model predicts a magnetic field strength of 16 G and height $\sim 10^5$ km at the position of depolarization, and the required density there was 6.4×10^7 cm^{-3}. The authors consider the resulting density too low to be compatible with simultaneous Faraday rotation observations (Alissandrakis and Chiuderi Drago, 1994) and concluded that the error could be due to the uncertainty involved in extrapolating field strengths all the way from the photosphere up to such high coronal heights.

Other studies have pointed out that some polarization observations appear to be incompatible with the most simple–minded applications of Cohen's (1960) theory (e.g., Gopalswamy, White, and Kundu, 1991; White, Thejappa, and Kundu, 1992). According to the theory, the mode coupling coefficient rapidly increases with frequency so that along a given line of sight mode reversal should occur at all frequencies below a certain transition frequency. In practice, however, polarization reversal is observed always to be absent at 1.5 GHz, even when it is present at 5 GHz. Gopalswamy et al. (1994) proposed that the theory for wave propagation through current sheets (Zheleznyakov, Kocharovsky, and Kocharovsky, 1996) may provide a possible explanation for these observations.

As noted above, exploitation of depolarization as a diagnostic requires that either the magnetic field or the density be known (allowing the other to be derived). In most of the studies mentioned above, the "known" quantity was either arbitrarily assumed, or based on a weak assumption such as a potential field extrapolation. We have available a well–tested magnetic field model for an active region which was observed by the VLA at several microwave frequencies. This data set therefore represents an excellent opportunity to explore the use of depolarization as a diagnostic. In addition to the availability of a better model for coronal magnetic fields than in previous applications, we use two well-separated frequencies in order to determine densities at two different coronal heights which allows us to investigate the vertical density structure. We also compare the results obtained with the "good" magnetic field model with results obtained from a potential field extrapolation, in order to address the model dependence of the density diagnostic. Thirdly, in addition to Cohen's theory in which rotation of magnetic field is the dominant effect, we investigate other effects such as the role of small scale density inhomogeneities (Melrose, 1985) and the presence of current sheets (Zheleznyakov and Zlotnik, 1988; Zheleznyakov, Kocharovsky, and Kocharovsky, 1996, 1984).

2. Mode Coupling Theories

In this section we briefly review the terminology of mode coupling theories (Cohen, 1960; Zheleznyakov and Zlotnik, 1964; see also Melrose, 1985). There are two fundamental quantities which play a role in mode coupling: the "polarization parameter", q, and the "mode coupling coefficient", Q. The polarization parameter is given by

$$q = \frac{f_B/2f}{1 - f_p^2/f^2} \, \frac{\sin^2\theta}{\cos\theta} \tag{1}$$

where f is the radio wave frequency, f_B and f_p are the gyrofrequency and the plasma frequency, respectively, and θ is the angle between the direction of wave propagation and the local magnetic field. The parameter q determines the polarization of the natural modes in the plasma, i.e., whether they are circularly polarized ($q \ll 1$) or linearly polarized ($q \gg 1$) at a given position along the ray path.

At each point along the propagation path of a ray, the radiation may be decomposed into a sum of components in the two natural modes (X and O) of the plasma. Since $q \ll 1$ except when $\theta \approx 90°$, the radiation is generally circularly polarized when emitted, and as long as $q \ll 1$, the natural modes are just the left– and right–circularly (hereafter, LC and RC, respectively) polarized modes and the two components may be thought of as propagating independently. However, if the radiation encounters a region where the natural modes are linearly polarized ($\theta \approx 90°$, $q \gg 1$), the circularly polarized emission must now be decomposed into the linearly polarized natural modes. When the coupling between the X and O modes is strong, the radiation fluxes in the X and O modes are exchanged; however, on either side of the layer, the line–of–sight magnetic polarity also reverses and the X and O modes switch their sense of circular polarization so that initial sense of polarization can be preserved. But when "weak" coupling applies, the radiation flux in each of the two natural modes does not change significantly even though the mode properties change dramatically, and since the X and O modes have opposite senses of circular polarization on either side of the layer in which $q \gg 1$, the overall polarization of the radiation reverses after it passes through the layer. The layer in which $q \ll 1$ (the magnetic field is transverse to the line of sight) is referred to as the quasi-transverse (QT) layer.

Mode coupling may occur when the refractive indices of the two modes are similar. At frequencies well above the resonant frequencies in the plasma, f_p and f_B, this only occurs when $q \approx 1$. The mode coupling coefficient Q may be understood in several ways, all of which amount to the same thing: one definition is the ratio of the characteristic length scale of the variation of q along the ray path to the scale over which the phase difference between the X and O modes is of the order unity (Zheleznyakov, Kocharovsky, and Kocharovsky, 1984, 1996). The latter scale is obviously large when the refractive indices of the two modes are similar, which corresponds to the limit of strong coupling between the two modes. Analytic expressions for Q may be evaluated for specific models of the layer in which $q \gg 1$. In Cohen's (1960) mode coupling theory, the primary change in mode properties (i.e. the change of q along a ray path) is due to rotation of the magnetic field direction. This model is based on the observation that q changes very rapidly with θ near $\theta = 90°$ (see eq. [1]). In this case the mode coupling coefficient for a ray path which crosses through the QT layer is:

$$Q_C \approx 0.2 f^4 f_B^{-3} f_p^{-2} L_\theta^{-1}, \tag{2}$$

where L_θ is the scale length for changes in the direction of the ambient magnetic field θ, and now all frequencies are in units of MHz and length scales in km.

An alternative to Cohen's model was provided by Melrose (1975), who considered the role of small–scale density inhomogeneities within the layers in which $q \approx 1$. In Cohen's theory the ray path is straight while the magnetic field direction changes from, say, $\theta < 90°$ to $\theta > 90°$. In Melrose's model, the ray path is not straight: the density inhomogeneities alter the local refractive index and thereby act to refract the ray. The distance over which the ray changes direction can be smaller than in Cohen's theory if the spatial scale of the inhomogeneities is small enough. Melrose (1975) obtains a coupling coefficient of

$$Q_M \approx Q_C + 0.2 f^2 f_B^{-3} L_N^{-1}, \tag{3}$$

where L_N is the length scale of the small-scale density inhomogeneities.

A quite different model invoking the presence of current sheets in mode coupling layer has been developed by Zheleznyakov and Zlotnik (1988) and Zheleznyakov, Kocharovsky, and Kocharovsky (1984, 1996) (see also Gopalswamy et al. 1994). In their model, the magnetic field at the center of the sheet is zero and the current density causes the component of **B** parallel to the sheet to reverse from one side to the other. Mode coupling in a current sheet is quite different from Cohen's model because the magnetic fields are anti-parallel on either side of the thin current sheet and the two modes become degenerate. Various forms of the mode coupling coefficient apply depending on detailed geometry of the current sheet and the magnetic field. It will suffice to note that strong coupling may occur if the change of magnetic field strength and mode properties across a current sheet with thickness L_s is rapid enough.

If these two parameters, q and Q, can be modeled, then we can predict the amount of change of the degree of circular polarization across a mode-coupling layer from the expression (Zheleznyakov and Zlotnik, 1964):

$$r_c \equiv V_{obs}/V_{int} = 2\exp(-\pi/2Q) - 1 \tag{4}$$

where V_{int} and V_{obs} are, respectively, the intrinsic and observed degree of circular polarization. Note that polarization reversal occurs when the coupling is weak ($Q \ll 1$); when the coupling is strong ($Q \gg 1$) mode identity changes (i.e. the X and O modes exchange their energy) which, however, results in preservation of circular polarization.

Complete depolarization ($r_c = 0$) occurs when $Q = \pi/2(\ln 2)$ (see Equation (4)). In this paper we apply this condition to derive densities by using observations of the location of the depolarization strips at different frequencies in conjunction with a state–of–the–art nonlinear force–free extrapolation of a photospheric vector magnetogram from which the coronal magnetic quantities (f_B, L_θ) at the heights corresponding to the observed depolarization strips can be obtained.

3. Observation

We show observational data in Figure 1. Figure 1(a) and (b) are the optical continuum and longitudinal magnetogram images of AR 6615 obtained at Big Bear Solar Observatory on 1991 May 7. In the continuum image (Fig. 1(a)) we number the sunspots for future reference. According to the magnetogram, the bipolarity in this active region is generally north-south (the magnetic neutral line is marked 'NL'); the three northernmost spots (labeled S1-S3) are of negative (going into the Sun) polarity while the other three spots (labeled S4-S6) are of positive polarity.

The radio observations of AR 6615 were made using the VLA[1] and have been discussed earlier by Lee et al. (1997ab). In the earlier studies our emphasis was

[1] The VLA is operated by the National Radio Astronomy Observatory, which is a facility of the National Science Foundation operated under cooperative agreement by Associated Universities, Inc.

on high spatial resolution, whereas here we are studying polarization and therefore emphasize sensitivity rather than spatial resolution. We therefore use conventional CLEANed images in the present analysis, rather than the "super-resolution" images employed by Lee et al. (1997a). Figures 1(c) and (d) show maps of the degree of polarization, $\rho_c = (T_R - T_L)/(T_R + T_L)$, at 4.9 GHz and 15 GHz, respectively. Here the white regions are dominated by RC polarization ($\rho_c > 0$) and the black, by LC polarization ($\rho_c < 0$). At both frequencies the noise level is of order 1% of the peak brightness temperature, and in order to avoid artifacts we calculate ρ_c only in regions where the local total intensity ($I = (T_R + T_L)/2$) exceeds 5% of its maximum. In these figures the photospheric neutral line ('NL') is shown as a solid line; depolarization strips at 4.9 GHz ('C') and at 15 GHz ('U') are shown as a dashed line and dot-dashed line, respectively. We note the following properties of polarizations at each frequency.

3.1. Depolarization at 4.9 GHz

At 4.9 GHz, negative polarization prevails over most of the active region. Unipolar microwave sources observed over bipolar active regions have also been reported by Schmeltz et al. (1994) and Alissandrakis et al. (1996). This is believed to happen when the inversion line shifts so far to one side (southward in the present case) that the QT surface covers the southern half of the active region and waves emitted from upgoing magnetic fields there, which start with intrinsic net positive polarity, reverse polarity on passing through the overlying QT surface. The emission from the northern half of the active region never encounters a QT surface, and consequently most of the active region appears to be LC polarized. The only two emission regions which are not LC polarized are seen in the south end (region A) and on the western side (region B).

Note that the degree of polarization is highest at the northern boundary of the active region and decreases monotonically from north to south until region A is reached. We tentatively conclude that the $V_{obs} = 0$ line seen in region A is due to depolarization. Since this line is a long way from the photospheric neutral line (in projection), the QT surface along the line of sight to A should be at a considerable height, where the density and magnetic field strength could well be low enough to allow strong coupling to occur (i.e., $Q_C \gg 1$ in eq. [2]).

The strong RC polarization observed in region B cannot be understood in the same way. This location is rather close to the photospheric magnetic neutral line, and so the waves emitted in region B would encounter the QT surface at much lower heights where the condition for strong coupling is unlikely to be satisfied.

3.2. Depolarization at 15 GHz

Due to the strong dependence of the mode coupling coefficient on frequency (see eqs. [2]–[3]) we expect that mode coupling at 15 GHz should be much stronger than that at 4.9 GHz along a given line of sight. This should have the effect of moving the depolarization strip much closer to the photospheric neutral line, which is entirely consistent with the pattern of polarization seen in Figure 1(d): at 15 GHz the depolarization strip (the dot-dashed line in Figure 1(d)) lies between the photospheric magnetic neutral line (solid line) and the depolarization strip found at 4.9 GHz (dashed line). We also note that the whole 15 GHz source over the southernmost sunspot, S4, is now RC polarized, implying that mode coupling in this region is strong enough to prevent a reversal. Observations of depolarization are rare at 15 GHz because the f^4 dependence of (2) tends to make mode coupling strong at high frequencies, but in this case the coronal magnetic fields are also quite strong, which has an opposing influence. For the purpose of density diagnostics, it is advantageous to compare depolarization strips at widely separated frequencies since they correspond to regions in the corona which are well–separated in height.

4. Predictions of Coronal Magnetic Field Models

We obtain coronal magnetic field models from field extrapolations of a vector magnetogram obtained with the Haleakala Stokes Polarimeter at Mees Solar Observatory. This magnetogram has low spatial resolution ($\sim 5''$), but does not saturate in the strongest fields in sunspot umbrae, which is essential for predicting coronal fields at large heights. In this paper we adopt a nonlinear FFF extrapolation for AR 6615 which has been found to provide a decent fit for the radio emission (Lee et al., 1997b). For comparison, we also use a potential field (PF) extrapolation in which currents are ignored: it is often argued that PF models should be adequate at large heights. In this paper, we avoid using *linear* FFF extrapolation for it might yield unrealistically strong magnetic fields at large heights (Alissandrakis, 1980). In the following we describe the properties of the QT surfaces and values of magnetic quantities based on the PF and FFF models, respectively.

4.1. Height variation of the QT surface

We proceed by defining horizontal planes at several discrete heights in the corona and determining the locus of the coronal neutral line on each plane. Figure 2 shows coronal magnetic neutral lines projected into the sky plane predicted by each model for heights of $h = 16''$, $33''$, $62''$, $98''$, and $140''$ respectively. Here the neutral line means the points where the magnetic field normal to the sky plane vanishes. Both the PF and the FFF predict a monotonic shift of the magnetic neutral line to the south as height increases in region A, consistent with the observed polarization (Section 3). In region B, the QT surface is doubly wrapped, i.e., a line of sight may cross the QT region in the corona twice. Such a doubly–wrapped feature has been seen in other observations as well (Schmeltz et al. 1994, Alissandrakis et al. 1996).

The QT surfaces resulting from the two magnetic models differ in (i) the slope of the QT surface in region A with respect to the line of sight, and (ii) the apparent position and width of the folded QT surface in region B. These differences originate from the built-in assumptions in each model regarding the boundary conditions and field extrapolation. In the FFF model, the QT surface is tilted more to the south than in the PF model, presumably due to the presence of coronal currents. Due to the sensitive form of (2), such differences in the geometry of the QT surfaces will lead to a significant difference in the electron densities derived from the depolarization condition.

4.2. Magnetic field strength and rotation length scale

Figure 3 shows vertical cross sections through the magnetic field model in the north–south direction, including the location of the QT surface, at $x = 423''$ (region A) and $x = 471''$ (region B). The contours in these figures represent isogauss surfaces with the field strength specified in units of gauss. The vertical straight lines are the observed projected positions of $\rho_c = 0$ in the C (5 GHz) and U (15 GHz) bands at the corresponding x–positions.

In region A (leftmost two panels in Fig. 3), the PF model predicts that the field strength and rotation length at the position of depolarization for 4.9 GHz are B = 5.3 G and $L_\theta = 2.0 \times 10^5$ km, while those at 15 GHz are 24 G and 1.0×10^5 km. By comparison, the FFF model produces much larger field strengths and much smaller scale lengths: 20 G and 7.1×10^4 km at 4.9 GHz and 56 G and 5.1×10^4 km at 15 GHz. Thus there is a large difference in the predicted field strength in the depolarization strips as well as the rotation length, and this greatly affects the densities inferred in the two models from the depolarization condition.

In region B (rightmost two panels in Fig. 3), both the FFF and the PF models predict a folded QT surface, but at different positions; under the action of currents, the QT region in the FFF model does not extend as far to the north as in the PF model. The field strength at the point $V_{obs} = 0$ (for 4.9 GHz only, since there is no 15 GHz emission in this region) is 14 G in the PF, but as large as 57 G in the FFF. Accordingly, in order to explain the observed polarization pattern in region B as due to depolarization, an implausibly low density $\sim 10^6$ cm^{-3} is required by the FFF model. It is thus unlikely that RC polarization in region B is explicable by adjusting densities.

4.3. The dipolar behavior of magnetic field strengths

It appears that in this active region the FFF model predicts much stronger field strengths in the QT layer than does the PF. This is not due to the fact that fields in the FFF are always stronger than those in the PF, but that along a given line of sight the FFF QT surface tends to be much lower in height (by a factor of 1.7) than the corresponding PF QT layer, under the action of currents. To clarify this point, we plot the field strength and rotation length scale at the QT surface for the two models in Figure 4. Here the cross symbols are field strengths that we read on the QT surface in the FFF model and the triangle symbols, in the PF model. Dotted lines indicate the heights we now concentrate on (4×10^4 km $< h < 1.2 \times 10^5$ km). In this limited height range, a good approximation for the dependence of B on height h in *both* models is $B(h) \sim h^{-3}$, i.e., a dipole–like height dependence, although considerable deviation from this dipole law is seen at lower heights (see Figure 4). The magnetic rotation length scale is approximately related to the height as $L_\theta(h) \approx (1.1 - 1.6) \times h$ in much of the active region. Since the field strength follows a similar dipole law at large heights in both models, it does not serve as a good discriminator between the models. The biggest difference between the two models in terms of the QT surface lies in the height of the QT surface rather than the field strength.

5. Mode Coupling

5.1. Depolarization due to rotation of magnetic fields

We now compare the observed inversion lines with those calculated from the magnetic models at the two frequencies. We first assume a plane parallel density model, parameterized by $N_e(h) = N_e^{\mathrm{o}} \exp[-h/H]$, with N_e^{o} and H being chosen so as to reproduce as closely as possible the observed locations of the depolarization strip at the two frequencies. Given N_e and $\mathbf{B}$, we can then calculate Cohen's mode coupling coefficient Q (eq. [3]) across the whole QT layer. Figure 5 shows the result as the ratio of the observed to the original circular polarization, r_c (eq. [4]). The morphologies of the r_c contours predicted by both models are similar, but there is a large difference between the two predictions in terms of the density required. Both models require a similar density at the base of the corona, $N_e^{\mathrm{o}} = 1.0 \times 10^{10}$ cm^{-3}, but widely different density scale heights: $H = 5.5 \times 10^4$ km for the PF model and 1.7×10^4 km for the FFF model, respectively.

The difference in density between the models increases with height due to the different scale heights, and reaches about two orders of magnitude difference at $h \sim 10^5$ km, i.e., $n_e = 2.8 \times 10^7$ cm^{-3} in the FFF model and $n_e = 1.6 \times 10^9$ cm^{-3} in the PF model. By comparison, the commonly-used quiescent coronal density model proposed by Papadopoulis and Kogut (1975), $n_e(h) \approx 6.7 \times 10^8$ cm^{-3} $\exp(-h/1.25 \times 10^5$ km), lies between the PF and FFF results. The density model required by the FFF QT layer predicts a density at 10^5 km which is similar to that obtained by Alissandrakis et al. (1996), which they regarded as being too low.

We also note that the theoretical depolarization strips (curves of $r_c = 0$ in Fig. 5) do not reproduce the observed $V_{obs} = 0$ line in region B very well. Since region B is close to the photospheric neutral line the QT surface lies at much lower coronal heights where the magnetic fields are strong, and with the density derived above the condition for strong coupling condition is never achieved. The fact that we nonetheless observe a polarity reversal there indicates that this model is not the appropriate explanation for region B.

5.2. Role of small-scale density inhomogeneities

In the previous section, we have found that with the more realistic of the two magnetic field models, the FFF model, the density required in the depolarization region is very small. Two possible reasons for such a result are (i) as suggested by Alissandrakis et al. (1996), the magnetic field extrapolation may not work well at large heights; or (ii) Cohen's mode coupling theory may be inadequate to describe the corona: it regards rotation of magnetic fields near $\theta \sim 90°$ as the primary cause for the rapid change of the polarization parameter q. If other contributions to the mode coupling coefficient are present, the density may actually be larger.

Melrose's (1975) theory for mode coupling (eq. [2]) provides such a case. In his theory, mode coupling is enhanced by the presence of small-scale density inhomogeneities. Figure 6 shows the effect on mode coupling of including such small–scale inhomogeneities in both magnetic field models. Densities along a selection of lines of sight are plotted, with lines connecting the densities in the 5 and 15 GHz depolarization strips. The dashed lines in this figure are results obtained using Cohen's theory alone, and the solid lines show the changes obtained by including the effects of inhomogeneities (eq. [3]). Papagianis and Kogut's (1975) density model is also shown as a thick solid line for comparison. Melrose's theory involves an additional free parameter which we cannot easily constrain at present: the length scale L_N of the inhomogeneities. In Figure 6 we have chosen values for L_N which produce a contribution to Q at least comparable to that of (2): as a guideline for this choice, we have attempted to achieve the same gradient in density with height as used by Papagianis and Kogut (1975). Because the magnetic field strength in the depolarization layer is very different in the two models, we have to use very different values for L_N: $L_N = 1000$ km in the PF model and $L_N = 20$ km in the FFF model. For simplicity, we have used the same value for L_N at both the 5 and 15 GHz depolarization heights. (The former value, in excess of $1''$, is rather large and cannot be regarded as "small–scale").

The notable feature of Figure 6 is that while it can result in a considerable change in the density required in the 5 GHz depolarization layer (the higher of the two layers), it has very little effect on the density required in the 15 GHz depolarization layer. This follows from the frequency–dependence of the mode coupling contributions: the term due to the inhomogeneities in (3) increases much less rapidly with frequency than Cohen's coefficient in (2), so that the coupling at high frequencies is generally dominated by Cohen's term while that at low frequencies is more controlled by the inhomogeneity term. There can only be a very narrow range of conditions in which both contribute similarly.

The major problem in interpreting the observations in terms of small–scale density inhomogeneities is that they must be sufficiently dense to cause refraction of the rays, and at the high frequencies we investigate here this requires unreasonably large densities: the refractive index is only substantially different from unity near the plasma frequency, which at 5 GHz requires a density of order 10^{11} cm^{-3}. (Melrose applied his theory to meter–wave emission, where the observing frequency is much closer to the plasma frequency at high altitudes in the corona.) Orrall et al. (1990) inferred sub-resolution density fluctuation from the EUV and K-coronal brightness which amounts to $\sqrt{\langle n^2\rangle/\langle n\rangle^2} < 6$ for an active region (see their table 3). This is still far below the amount of density fluctuation we would need here. Therefore, we conclude that it is unlikely that small–scale inhomogeneities play a role in mode coupling in these data.

5.3. RC–polarization in region B

We noted earlier that in region B the QT surface has a fold (Figure 2 and 3). The bottom edge of this fold is at an altitude of order 7000 km in the FFF model, and 15000 km in the PF model. Any emission which originates below these heights may pass through the QT surface twice. Based on the field strengths shown in Figure 3, the 4.9 GHz emission will originate below the QT surface (no 15 GHz emission is observed from this location). From the extrapolations it is apparent that the direction of the magnetic field in the emission region should favor the production of LC polarized emission. Since it is likely that weak coupling should apply to both QT surfaces, the polarization of the radiation should reverse at each surface and result in an observed net LC polarization, whereas the opposite polarity is observed. In this section we check the possibility that some other effect may be playing a role in this region.

One instrumental effect which must be considered is that of "beam squint" in the VLA antennas. This arises from the fact that the VLA has off–axis feeds with distinct RCP and LCP receivers, resulting in the two polarizations having slightly different centers for their primary beams (e.g., Vourlidas and Bastian, 1994). The offset between the polarized beams and the phase center of the observation is about 3% of the half–power width of the primary beam. Near phase center the two beams have essentially identical responses, but at the edge of the primary beam where sensitivity falls off rapidly, the difference between the intrinsic responses of the two polarizations can be large and this can cause unpolarized sources to appear to have significant polarization. However, region B lies about $100''$ from the phase center of the observation, which is at about the 95% response level at 5 GHz. Thus the difference in response of the two polarized beams should be at most of order a few percent and cannot explain the large degree of positive polarization observed in region B; in addition, the observed pattern is not consistent with the effect of beam squint.

Even if the emission region lies above the lower fold of the QT surface we would still expect to observe LC polarization because the source should then be intrinsically RC polarized and the radiation will cross the QT surface only once en route to us.

The fact that there is a QT region so low over region B offers the possibility that the magnetic environment there is somewhat peculiar. Specifically, the emission may originate in the QT region itself, rather than a region where the natural modes are circularly polarized as is usually the case. In Figure 7(a) we plot the polarization parameter q and the degree of circular polarization $(T_R - T_L)/(T_R + T_L)$ along a line of sight in region B at $(x, y) = (471'', 260'')$. The latter was calculated using the Ratcliff's (1959) formula assuming an original polarization of $(T_X - T_O)/(T_X + T_O) = 1/4$: here we are only interested in showing how the polarization changes with propagation. Based on this calculation, it appears that even at very low heights near the magnetic neutral line the limit of circularly–polarized natural modes ($q \ll 1$) applies.

An alternative explanation is that the original polarization of the emission in region B was not X mode (corresponding to LCP) but rather O mode. Circumstances in which intrinsic O mode polarization may occur have been discussed: for gyroresonance emission, this usually requires that the X and O modes come from different harmonic layers. If both modes are optically thick but the O mode layer has a higher temperature, then net O mode polarization will result (e.g., Zlotnik, 1993; Vourlidas, Bastian, and Aschwanden, 1996; White and Kundu 1997). However this scenario for O mode polarization is not possible for the source in region B, where emission angles are large and the difference in opacity between the two modes is therefore small: both modes would be expected to originate in the same harmonic layer.

The last alternative that we mention is that one of the folds in the QT surface actually contains a thin current sheet. In such a thin current sheet, strong rather than weak coupling generally takes place (Zheleznyakov and Zlotnik, 1988; Zheleznyakov, Kocharovsky, and Kocharovsky, 1984, 1996). Our magnetic field data do not have sufficient spatial resolution to address this question, since the current sheets are likely to be on subarcsecond spatial scales. To explore the possibility of why such a current sheet should exist (if it does at all) in region B rather than the other regions, we show, in Figure 7(b), the field line geometry in region B. The field lines here are mostly transverse and the polarity changes rapidly with height. This is due to the fact that magnetic flux from S4 and S6 compete against S3 (see Figure 1 and 2). As a result the field configuration in this region features a system of two layers with oppositely directed magnetic fields, which is the classic geometry for a current sheet. Specifically, the grey colored bar in Figure 7(b) is the location where the current sheet is most likely to be present. Region B is the only place in this active region which contains such a change of magnetic field direction over short distances. Thus it is not implausible that a current sheet could exist at low altitudes in this region.

Note, however, that the obvious location for such a current sheet, while it does intersect the QT region, is not coincident with it. Since the current sheet preserves the incoming polarization, it will not affect the observed polarization anywhere except at the one line of sight which passes though the point of intersection between the current sheet and the QT region. On either side of this intersection point the lines of sight still pass though the QT layer twice, as well as through the current sheet, and the original polarization should be preserved. Since the point of intersection between the very narrow current sheet and the narrow QT layer is so small compared to the size of region B, we conclude that a current sheet is unlikely to be the explanation for the observed polarization there.

6. Discussion and Conclusion

In this paper we have taken advantage of the availability of both excellent magnetic field data and excellent radio observations of depolarization to investigate the use of mode coupling as a coronal diagnostic. In the context of Cohen's theory, comparison of the magnetic field model with the observed polarization should yield a straightforward density measurement. Our analysis has encountered two difficulties: (i) the density derived for heights of order 10^5 km ($\approx 3 \times 10^7$ cm^{-3}) is lower than other plausible estimates; and (ii) the polarization in region B is not consistent with the magnetic field data.

The inference of either a low density when the magnetic field model is specified, or equivalently a low magnetic field strength when the density is specified, has been a common complaint of studies which have employed the depolarization condition as a diagnostic (e.g., see White et al. 1992 for a review). Alissandrakis et al. (1996) attribute the inference of low densities to uncertainties in the extrapolation of photospheric fields to large coronal heights, and our comparison of the PF and FFF models clearly indicates that this is an important issue. We have carried out some additional tests and find that the omission of weak fields from the boundary of a region has relatively little effect on the location of the QT layer, whereas any errors in the measurement of strong sunspot fields (such as may result if a filtergram-based magnetogram is used which saturates in the umbrae of strong sunspots is used as a boundary condition) have a large effect. We believe that the strong umbral fields are well determined in the present data.

In our results, the sensitivity of the diagnostic results to the input magnetic field model arises not because different models produce very different magnetic field *strengths* at the same height, which is not true: rather, it is because the two models predict quite different QT surfaces. In regions where the QT surface is nearly vertical, a relatively small horizontal displacement in the QT surface produces a huge difference in the height of the point of intersection between the QT surface and a given line of sight, and this difference in height produces a large difference in the magnetic field strength in the location where depolarization should occur. In the present case, there is a difference between the two models by a factor of 1.7 in the height of the QT layer along a given line of sight. With field strength roughly obeying a dipole variation with height, the difference in density inferred in the two models at a fixed value of Q is of order $n_e \sim B^{-3} L_\theta \sim h^8 \sim (1.7)^8 \sim 70$. The fact that we inferred a very small scale height for density using the FFF model is due to the rapid decrease of field strength with height. Despite the sensitivity of Q to frequency f and the availability of two well–separated frequencies, the decrease of f_B with height easily offsets the contrast in frequency. These problems could not have been appreciated in previous studies where either a single frequency or a single magnetic field model was used in the analysis of polarization data.

We were also unable to explain the presence of RC polarization surrounded by LC polarization in region B. We cannot simply dismiss this observation as due to the inaccuracy of our models because, as noted, if we change the intrinsic polarization of the emitted radiation then the QT surface will no longer show a fold, and consequently the radiation should still appear to be RC polarization. This region contains a magnetic configuration which seems ideal to result in a current sheet which can affect the observed polarization (Zheleznyakov, Kocharovsky, and Kocharovsky, 1984, 1996), but the logical position of this current sheet does not exactly coincide with the QT layer and consequently cannot explain the width of the observed RC polarized feature.

Acknowledgements

This work has been supported by NSF grant ATM-93-16972 and NASA grant NAG-W-1541. Z. M. has been supported by NASA contract NASW-4728 and NSF grant ATM-9320575. A. N. M. has been supported by ATM 93-20575 and ATM 96-13794. We thank R. Fear for providing the BBSO data.

References

Alissandrakis, C. E.: 1981, *Astron. Astrophys.* **100**, 197.
Alissandrakis, C. E., Borgioli, F., Chiuderi-Drago, F., Hagyard, M., and Shibasaki, K.: 1996, *Solar Phys.* **167**, 167.
Alissandrakis, C. E. and Chiuderi-Drago, F.: 1994, *Astrophys. J.* **428**, L73.
Cohen, M. H.: 1960, *Astrophys. J.* **131**, 664
Gopalswamy, N., Zheleznyakov, V. V., White, S. M., and Kundu, M. R.: 1994 *Solar Phys.* **155**, 339.
Gopalswamy, N., White, S. M., and Kundu, M. R.: 1991, *Astrophys. J.* **379**, 366.
Kundu, M. R. and Alissandrakis, C. E.: 1984, Solar Phys. 94, 249.
Lee, J., White, S. M., Gopalswamy, N., and Kundu, M. R.: 1997a, *Solar Phys.* **174**, 175.
Lee, J., McClymont, A. N., Mikić, White, S. M., and Kundu, M. R.: 1997b, *Astrophys. J.* , submitted.
McClymont, A. N., Jiao, L., and Mikić, Z.: 1997, *Solar Phys.* **174**, 191.
Melrose, D. B. 1985, in Solar Radiophysics, D. J. McLean and N. R. Labrum (eds), Cambridge University Press.
Melrose, D. B.: 1975, *Solar Phys.* **43**, 79.
Orrall, F. Q., Rottman, G. J., Fisher, R. R., and Munro, R. H.: 1990, *Astrophys. J.* **349**, 656.
Papagianis, M. D. and Kogut, J. A.: 1975, AFCRL-TR-75-0430.
Ratclliff, J. A.: 1959, The Magneto-ionic Theory and its Application to the Ionospheric Atmosphere, p. 206, Cambridge University Press.
Schmelz, J. T., Holman, G. D., Brosius, J. W., and Wilson, R. F.: 1994, *Astrophys. J.* **434**, 786.
Voulidas, A., Bastian, T. S., and Ashwanden, M. J.: 1996, *Bull. American Astron. Soc.* **188**, #36.02.
Vourlidas, A. and Bastian, T. S. 1994, VLA Test Memorandum 180.
White, S. M., Thejappa, G., and Kundu, M. R.: 1992, *Solar Phys.* **138**, 163.
White, S. M. and Kundu, M. R.: 1997, *Solar Phys.* **174**, 31.
Zheleznyakov, V. V. 1970, *Soviet Astron.* **6**, 3.
Zheleznyakov, V. V. 1962, *Soviet Astron.* **6**, 3.

Zheleznyakov, V. V. and Zlotnik, E. Ya. 1988 , *Soviet Astron. Letters* **14**, 73.
Zheleznyakov, V. V. and Zlotnik, E. Ya. 1964, *Soviet Astron.* **7**, 485.
Zheleznyakov, V. V., Kocharovsky, V. V., and Kocharovsky, Vl. V.: 1996, *Astron. Astrophys.* **308**, 685.
Zheleznyakov, V. V., Kocharovsky, V. V., and Kocharovsky, Vl. V.: 1984, *Soviet Phys. Usp.* **26**, 877.
Zlotnik, E. Ya. 1968, *Soviet Astron.* **12**, 245.
Zlotnik, E. Ya. 1993, private communication.

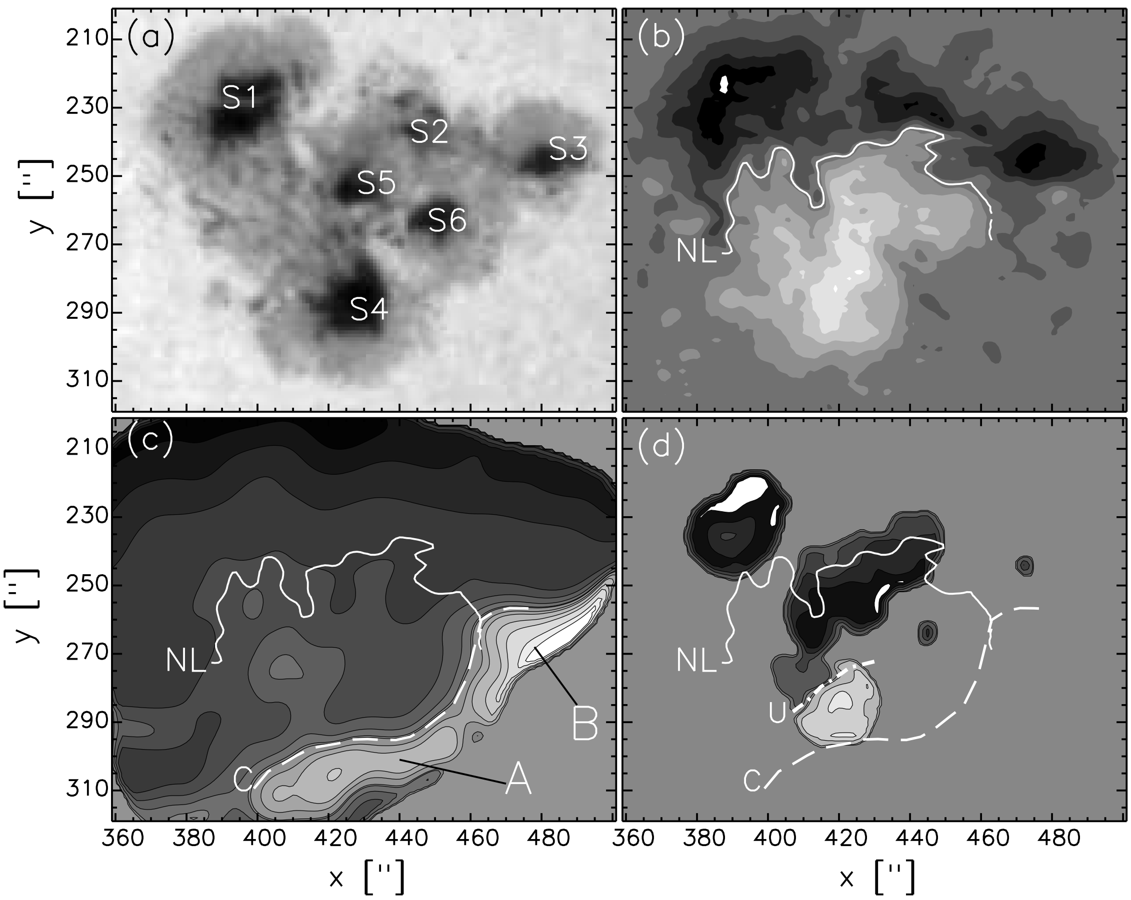

Figure 1. (a) A white-light picture of AR 6615. The major sunspots are labeled S1–S6. (b) A longitudinal magnetogram of AR 6615. The photospheric magnetic neutral line is marked by a white solid line ('NL'). These two images were kindly provided by Big Bear Solar Observatory. (c) The degree of circular polarization at 4.9 GHz. The bright filled contours represent RCP polarization and the dark filled contours, LCP polarization. Contour levels are at [-90, -70, -50, -30, -10,-6, -3, -1, 1, 3, 6, 9, 15, 20] %. The depolarization strip appears in between the L polarized region in the north and the R polarized regions, A and B, in the south. x and y are geocentric coordinates in the west and the southern hemisphere, respectively. (d) The degree of circular polarization at 15 GHz. Contour levels are [-90, -70, -50, -30, -10,-5, 5, 10, 30, 50, 70] %. The dot-dashed line ('U') and dashed line ('C') are the depolarization strips identified at 15 GHz and 4.9 GHz, respectively. In both radio images the degree of polarization is only plotted in regions of significant emission.

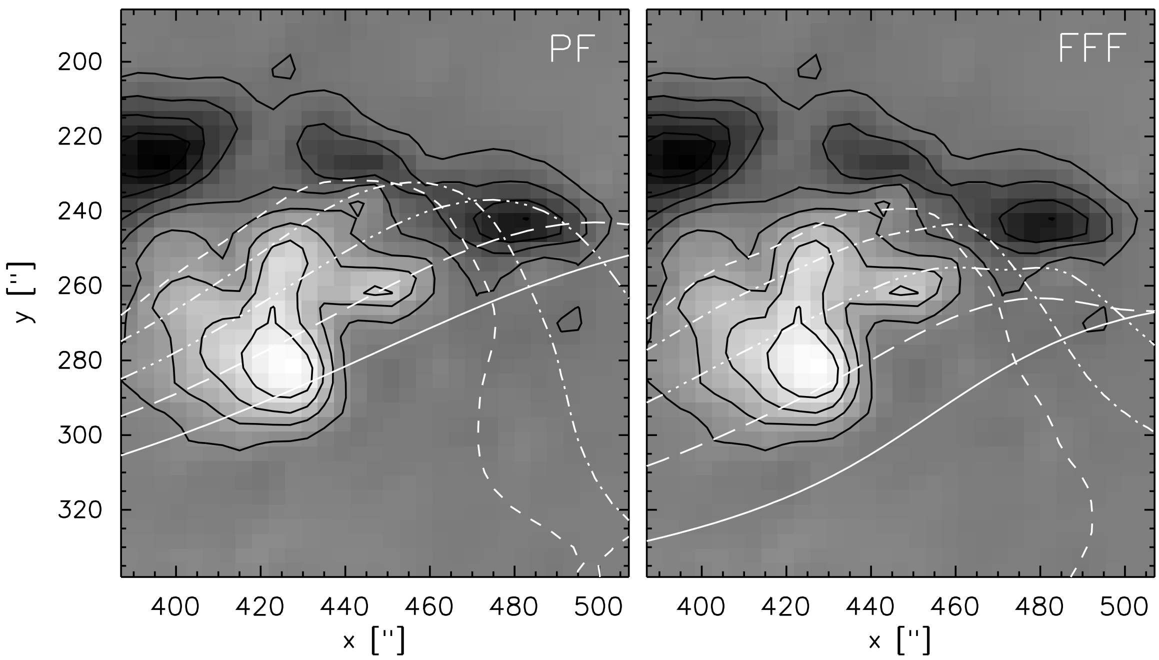

Figure 2. The coronal magnetic neutral lines (white lines) predicted by the PF (left panel) and the FFF (right panel) models, respectively, overlaid on the photospheric magnetogram (greyscale images with black contours). The neutral lines are projected onto the photosphere and correspond to heights of $h = 16''$ (short dashes), $33''$, $62''$, $98''$, and $140''$ (solid line), with height increasing from top to bottom at the left edge of each panel.

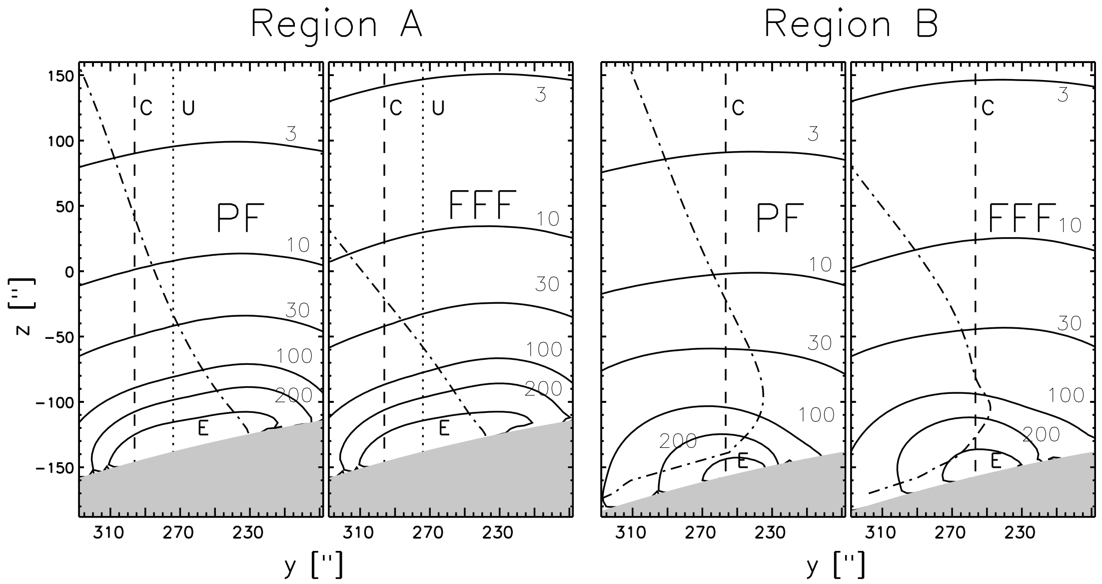

Figure 3. Vertical cuts through the corona showing the locations of the QT surface in regions A and B. The leftmost two panels show the locations of the QT surface (the dot-dashed lines) in the y-z plane corresponding to $x = 423''$ (region A) as predicted by the PF and the FFF models, respectively; the rightmost two panels are the same for region B ($x = 471''$). Contours are isogauss surfaces at the field strengths specified in units of gauss. The contour marked as 'E' is the 430 G surface which we presume to be the emission layer for 4.9 GHz. The vertical lines marked C and U represent the $y-$position of the observed depolarization strip at the $x-$position shown. The filled region at the bottom of each panel is the solar surface.

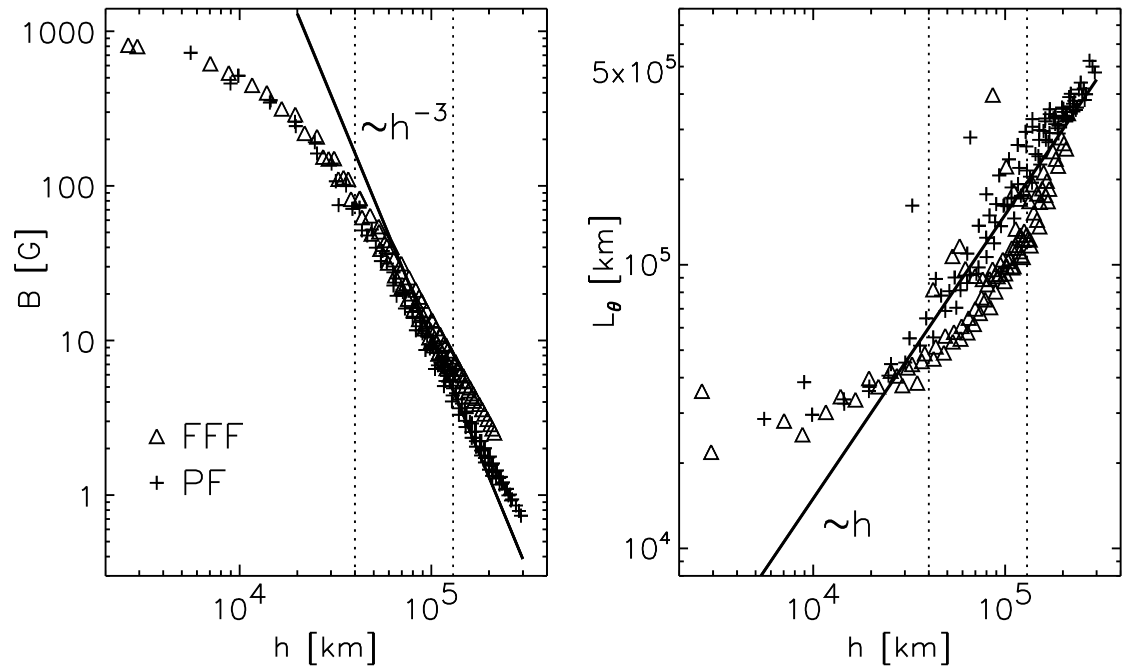

Figure 4. (a) The field strength, B, and (b) the length scale of magnetic field rotation, L_θ, on the QT surface as a function of height, h. The thick solid lines are rough fits to the relationship between B and h or between L_θ and h within the height range of interest here (shown by the vertical dotted lines).

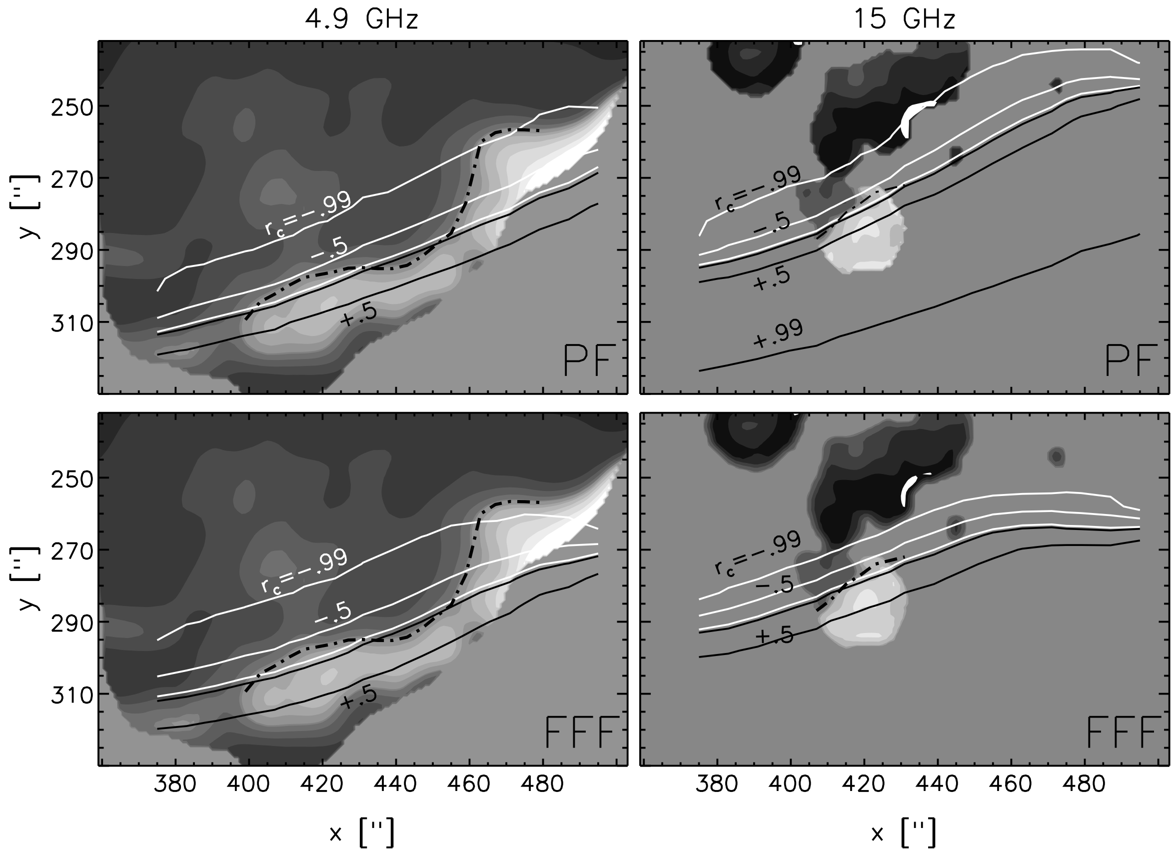

Figure 5. Theoretical mode conversion factors $r_c = V_{obs}/V_{int}$ (solid line contours) overlaid on the observed degree of polarization at the two frequencies (greyscale images). r_c in the upper two panels is calculated using the PF and in the lower two panels using the FFF model. The densities used were chosen to get the calculated depolarization strip match the observed depolarization region as closely as possible. These are: $n_e(h) = 1.02 \times 10^{10} \exp[-h/5.5 \times 10^4 \text{ km}]$ for the PF model and $n_e(h) = 1.03 \times 10^{10} \text{ cm}^{-3} \exp[-h/1.7 \times 10^4 \text{ km}]$ for the FFF model. The white and black contours represent $r_c = \pm 0.99$, $\pm .5$, and $\pm .05$, respectively.

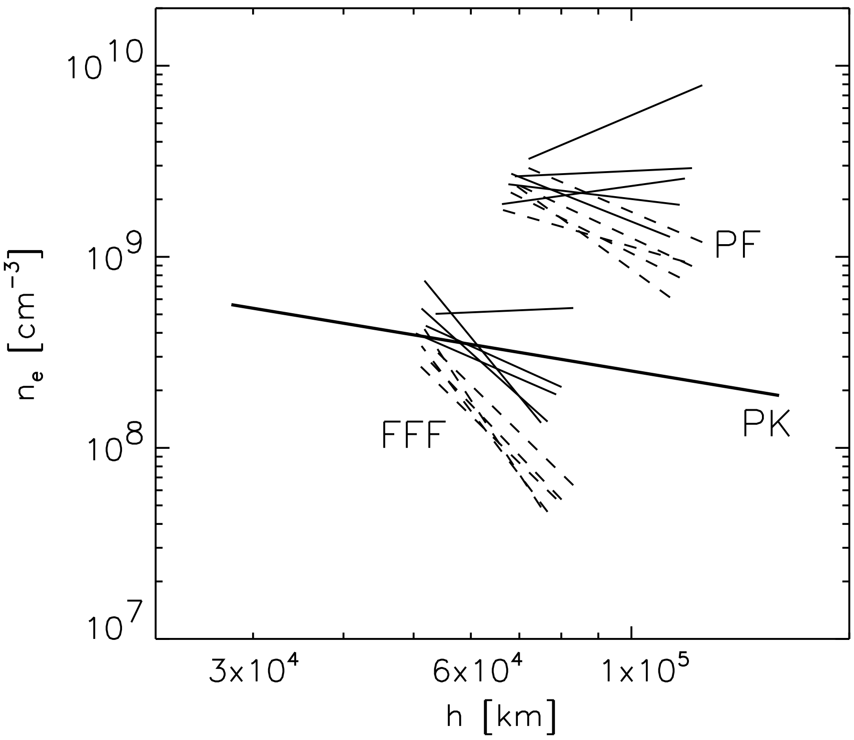

Figure 6. Inferred coronal densities as a function of height. The dashed lines connect densities inferred at the depolarization strips at 4.9 GHz to those at 15 GHz using Cohen's (1960) mode coupling coefficient. The solid lines are the results obtained using Melrose's (1975) expression with $L_N = 1000$ km for the PF model and $L_N = 20$ km for the FFF model . The thick solid guide line marked 'PK' refers to the coronal density model of Papagianis and Kogut (1975).

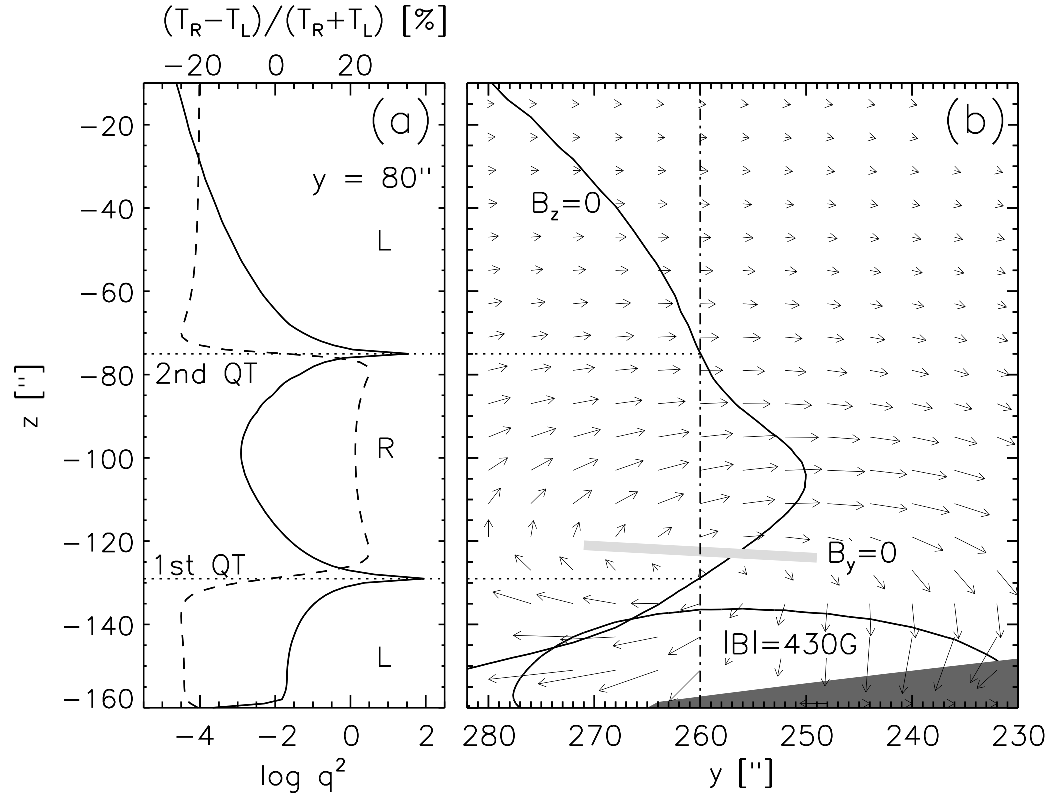

Figure 7. Wave propagation in region B. (a) The solid line represents the polarization parameter, q, while the dashed line is the degree of circular polarization along the line of sight z at $(x, y) = (471'', 260'')$. (b) Arrows represent magnetic field vectors in the y–z plane at $x = 471''$; the curves marked '$B_z = 0$' and '$|B|$=430G' are, respectively, the QT surface and the fourth harmonic emission layer at 4.9 GHz. The grey colored bar marked '$B_y = 0$' is the proposed location of the current sheet. The vertical dashed line corresponds to the line of sight used in (a).